Polímeros
ISSN 1678-5169 (Online)

https://doi.org/10.1590/0104-1428.20250044

ORIGINAL ARTICLES

UV exposure analysis on mechanical resistance of rope yarns for offshore mooring*

Daniel Magalhães da Cruz[1,2]*, Marcelo de Ávila Barreto[2,3], Larissa Basei Zangalli[2], Felipe Tempel Stumpf[1], Carlos Eduardo Marcos Guilherme[3], Ivan Napoleão Bastos[4] and Ana Lúcia Nazareth da Silva[5,6]

[1]Grupo de Mecânica Aplicada – GMAp, Programa de Pós-graduação em Engenharia Mecânica – PROMEC, Universidade Federal do Rio Grande do Sul – UFRGS, Porto Alegre, RS, Brasil

[2]Tecnofibers Desenvolvimento e Tecnologia Ltda., Itajaí, SC, Brasil

[3]Laboratório de Análise de Tensões Policab, Programa de Pós-graduação em Engenharia Mecânica – PPMec, Universidade Federal do Rio Grande – FURG, Rio Grande, RS, Brasil

[4]Laboratório de Corrosão – LabCor, Instituto Politécnico da Universidade do Estado do Rio de Janeiro – IPRJ, Universidade do Estado do Rio de Janeiro – UERJ, Nova Friburgo, RJ, Brasil

[5]Instituto de Macromoléculas Professora Eloisa Mano – IMA, Universidade Federal do Rio de Janeiro – UFRJ, Rio de Janeiro, RJ, Brasil

[6]Programa de Engenharia Ambiental – PEA, Universidade Federal do Rio de Janeiro – UFRJ, Rio de Janeiro, RJ, Brasil

**daniel.cruz@ufrgs.br*

** This paper has been partially presented at the 17th Brazilian Polymer Congress, held in Joinville, SC, 29/Oct - 02/Nov/2023.*

Abstract

Polyester (polyethylene terephthalate, PET) and high-modulus polyethylene (HMPE) fibers are currently among the most commonly used materials in the manufacturing of ropes for offshore operations. Several studies have been conducted in analytical, experimental, and numerical domains, addressing various factors such as tensile tests, fatigue, creep, and environmental exposure conditions that influence their mechanical behavior. This work presents data from an experimental study on rupture resistance in semi-finished products (rope yarns) of PET and HMPE fibers subjected to different ultraviolet (UV) radiation exposure durations. The experimental procedure involved UV exposure for up to 84 days, followed by tensile rupture tests based on ISO 2062. The results showed that UV degradation occurs in a monotonic manner for PET, whereas HMPE exhibits relative stability for rope yarns.

Keywords: *experimental characterization, offshore applications, polymeric fibers, strength at break, ultraviolet degradation.*

Data Availability: Research data is available upon request from the corresponding author.

How to cite: Da Cruz, D. M., Barreto, M. A., Zangalli, L. B., Stumpf, F. T., Guilherme, C. E. M., Bastos, I. N., & Silva, A. L. N. (2025). UV exposure analysis on mechanical resistance of rope yarns for offshore mooring. *Polímeros: Ciência e Tecnologia*, *35*(4), e20250043.

1. Introduction

The adoption of polymeric fibers in offshore mooring systems began in the 1990s with Del Vecchio's pioneering proposal to replace steel lines with synthetic ropes[1]. This shift enabled the transition from catenary to Taut-Leg systems, offering benefits such as lower weight, easier installation, improved dynamic response, greater corrosion resistance, and more efficient offshore deployment[2-7]. Since then, polymeric fibers have evolved from an alternative to a key component in offshore mooring and other marine applications[8-10].

Polyester (PET) is the most widely used fiber in mooring ropes, valued for its mechanical performance, ease of processing, dimensional stability, recyclability, and especially its low cost[5,10-13]. Its broad availability and industrial maturity also reinforce its dominance[14]. However, growing offshore demands have driven the adoption of alternative fibers such as polyamide, aramid, and high-modulus polyethylene (HMPE)[9,10,15,16].

Each fiber has found its niche in specific applications: polyamide, with high energy absorption, is used in shallow-water mooring and Single Point Moorings (SPM)[17-19]; aramid and HMPE, with high specific strength, are common in nautical ropes, towing lines, and structural offshore components requiring lightness and strength[20-22].

In permanent offshore mooring, HMPE has recently gained attention as an alternative to polyester, due to its low elongation (suitable for deeper waters), high tensile strength, and tenacity—classifying it as a high-performance fiber[23-26]. The development of low-creep HMPE and advances in production (reducing costs) further boost its offshore potential[27,28].

Beyond mechanical performance, the durability of synthetic fibers in marine environments is crucial for their selection and use. Alongside static and cyclic loads, environmental factors like abrasion, temperature changes, seawater immersion, and ultraviolet (UV) radiation can significantly impact long-term fiber integrity[29-33]. UV exposure is especially critical in top-line regions, where direct sunlight accelerates degradation and reduces mechanical properties[34-36].

Several studies have investigated the effects of UV radiation on synthetic fibers used in different applications, analyzing parameters such as mass loss, morphological changes, and tensile strength reduction. Said et al.[37] examined Ultra Long Duration Balloons (ULDB), where films act as gas barriers and fiber tendons provide structural strength. Their results showed significant strength loss in most fibers after UV exposure, except for Spectra®, which exhibited superior stability. Flory and Banfield[38] focused on synthetic ropes in offshore environments, addressing myths and facts about sunlight-induced degradation. They found LCP fibers highly sensitive to UV, while polyester and HMPE showed greater stability. The study also noted that rope color affects UV susceptibility and that larger-diameter ropes tend to suffer less UV damage than thinner ones.

Sørensen et al.[39] examined UV degradation in natural and synthetic microfibers, including combined effects of UV and seawater exposure. Polyamide showed notable surface changes without fragmentation, while PET and wool exhibited both surface damage and fragmentation, indicating chain scission. Da Cruz et al.[40] evaluated UV effects on the tensile strength of multifilaments used in offshore mooring. After up to 28 days of exposure, polyamide and polyester showed high stability, aramid and HMPE moderate degradation, and LCP significant mechanical loss. Del Vecchio et al.[41] investigated replacing top chains with synthetic ropes in mooring systems, noting that UV effects must be considered near the surface. Braided covers with internal filters offered effective protection, though small-diameter ropes with thinner layers allowed greater UV penetration.

In this context, the present study proposes an experimental approach to analyze UV aging in synthetic rope yarns—twisted but unbraided structures one level above multifilaments in the mooring rope hierarchy, as shown in Figure 1[42]. This setup facilitates understanding mechanical behavior under UV exposure and comparing fiber types. HMPE and PET samples underwent Type A ultraviolet exposure cycles for up to 84 days under controlled lab conditions. After exposure, standardized rupture tests assessed breaking strength, while stress-strain and tangent modulus curves were also obtained.

With this approach, the study aims to improve understanding of UV radiation effects on synthetic fibers used in offshore mooring, providing technical insights for selecting, sizing, and predicting the service life of ropes in harsh environments.

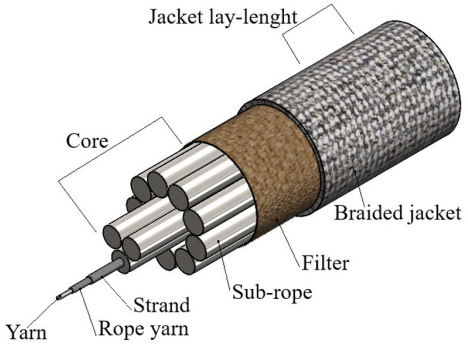

Figure 1. Schematic structure of an offshore mooring rope[42].

The comparative results between materials, along with their agreement or divergence from existing literature, may also guide future research.

2. Materials and Methods

2.1 Fiber information and rope yarn construction

The materials tested for ultraviolet aging were semi-finished products (SFP) or rope yarns made from high-modulus polyethylene (HMPE) and polyester (PET) fibers. For HMPE, 7 yarns with a linear density of 1760 dtex, each containing 480 filaments, were used; the manufacturer yarn code is JX99 1600D/480f. For PET, 19 yarns with a linear density of 2200 dtex, each with 192 filaments, were used; the manufacturer yarn code is SFS5202 2200dtex/192f.

The rope yarns were twisted to a ratio of 60 turns per meter for both HMPE and PET samples, using industrial rope-making twist equipment. These semi-finished products are commercial-grade constructions typically employed as protective jackets in offshore mooring ropes. The selected configurations (7 HMPE yarns and 19 PET yarns), were chosen to produce similar rope yarn diameters compatible with the twisting process for both materials, while also maintaining a comparable total filament count (3360f for HMPE and 3648f for PET). This balance ensured consistent manufacturability and handling during fabrication. Due to confidentiality agreements with the supplier, the manufacturer's name and the specific twisting apparatus cannot be disclosed, although the provided twist density enables reproduction of the rope yarn structure.

Semi-finished products, or rope yarns, are made from multifilaments drawn from untwisted spools and come with a manufacturer-provided test report, as shown in Table 1. Figure 2 displays the single multifilament spools for HMPE and PET, along with coils of the final rope yarn samples for both fibers

Both fibers studied are intended for offshore use but differ significantly in cost: HMPE at approximately 17.50 USD/kg and PET at 3.20 USD/kg. The test report at the multifilament level (Table 1) show elongation values consistent with literature[15,16,40,43,44], with HMPE rupture strain below 4% and PET rupture strain between 11% and 14%. Linear tenacity values in Table 1 are also notable.

(a) (b) (c)

Figure 2. Material fibers: (a) HMPE multifilament spool; (b) PET multifilament spool; (c) HMPE and PET rope yarns for UV aging.

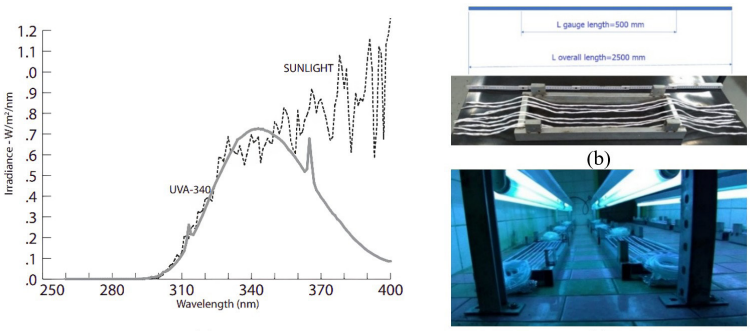

(a) (b) (c)

Figure 3. Ultraviolet exposure: (a) wavelength of UVA-340 lamp[47]; (b) samples in the apparatus and lengths; (c) exposure of samples.

Table 1. Test report results for single yarns used in constructions of rope yarn samples.

Material	HMPE		PET	
Properties	**Technical Standard**	**Testing Results**	**Technical Standard**	**Testing Results**
Linear density [dtex]	1777±124	1769	2240±45	2262
Force at break [N]	≥551.1	597.9	≥180	189
Strain at break [%]	≤4.0	3.5	14.0±2.0	13.9
Linear tenacity [cN/dtex]	≥31	33.8	≥8.2	8.3

HMPE results comply with ISO 18692-3[45], which requires a minimum linear tenacity of 2.5 N/tex. And PET values meet ISO 18692-2[46], specifying a minimum linear tenacity of 0.78 N/tex.

2.2 Ultraviolet exposures

UV exposure tests were conducted at the Polytechnic Institute of the State University of Rio de Janeiro in Nova Friburgo. A Q-Lab UVA-340 ultraviolet lamp[47] was used, simulating sunlight in the critical short-wavelength range of 295-365 nm, peaking at 340 nm with irradiance between 0.68-0.89 W/m²/nm (Figure 3a[47]). Five rope yarn samples were tested for each UV exposure condition.

The sample holder and sample length are shown in Figure 3b. Areas outside the analysis region were covered with aluminum foil to block UV radiation. Figure 3c depicts the UV exposure setup, with the lamp positioned 150 mm from the samples. Exposure times were 0 (without exposure), 14, 28, 42, 56, 70, and 84 days. Samples were rotated halfway through each exposure period to ensure uniform irradiation, as detailed in Table 2.

Table 2. Ultraviolet exposure times: withdraw and rotation samples, HMPE and PET.

Time [days]	Date (dd/mm/yyyy)	Event
0	10/05/2022	Sampes without exposure
7	17/05/2022	Rotation 14 days
14	24/05/2022	Withdraw 14 days & rotation 28 days
21	31/05/2022	Rotation 42 days
28	07/06/2022	Withdraw 28 days & rotation 56 days
35	14/06/2022	Rotation 70 days
42	21/06/2022	Withdraw 42 days & rotation 84 days
56	05/07/2022	Withdraw samples 56 days
70	19/07/2022	Withdraw samples 70 days
84	02/08/2022	Withdraw samples 84 days

2.3 Mechanical characterization

Mechanical characterization of the rope yarns was performed at the Policab Stress Analysis Laboratory, Federal University of Rio Grande, Brazil. Tensile strength tests covered all seven UV exposure conditions in Table 2 and followed ISO 2062[48]. Samples were 2500 mm long for handling and gripping (Figure 4a), with an effective gauge length of 250 mm between grips. For each UV condition, 5 specimens twisted at 60 turns per meter were tested to rupture using Instron 8801 servohydraulic testing machine (Figure 4b), recording force [N] and strain [%] continuously. A constant extension rate of 250 mm/min was applied until break.

An additional set of unexposed specimens (10 per material) was tested for linear density (ρ_L) per ASTM D1577[49] using a precision balance (Figure 4c). This allowed calculation of linear tenacity values for HMPE and PET without UV exposure. All mechanical tests after UV exposure were conducted under ISO 139[50] standard temperature and humidity conditions. Figure 4d shows an SFP specimen mounted in the testing machine before rupture.

2.4 Statistical filtering and data analysis

Before analyzing and interpreting the experimental results, appropriate filtering and statistical tests were applied to improve data reliability and consistency[51]. This step minimizes the influence of outliers and strengthens the robustness of the study's conclusions. In experiments involving synthetic polymeric fibers, statistical treatment is especially important due to the inherent variability linked to their viscoelastic behavior[52]. Nevertheless, Boiko et al.[53] note that, under controlled conditions, many of these materials tend to show an approximately normal distribution in their mechanical response.

Thus, individual data points for rupture force and strain were filtered using the statistical software Orange[54], applying outlier detection via boxplot analysis, the Ryan-Joiner normality test, Levene's test for homogeneity of variance, and one-way ANOVA. All tests were performed with a significance level of $\alpha = 0.05$, indicating a probability of incorrectly rejecting the null hypothesis (H_0), which corresponds to a Type I error.

With the filtered data following ultraviolet exposure, the initial analysis presents raw rupture force and strain values plotted against UV exposure time. Normalized values, relative to the unexposed condition, are also considered. To model the behavior of rupture force or strain over time, mathematical fitting using linearization and the method of least squares (MLS)[55] are applied, with the coefficient of determination serving as the criterion for model selection.

Beyond rupture data, the full constitutive behavior during tensile testing is captured in terms of force and strain. To represent this, a stress-strain curve is constructed. However, directly applying the conventional stress definition (force over cross-sectional area) is impractical due to the difficulty in accurately measuring the area of fiber bundle. Instead, a mathematical approach from the literature[40,56] is used, where stress (σ) is calculated from rupture force (F), linear density (ρ_L), and material density (ρ), as shown in Equation 1.

$$\sigma\left[\text{MPa}\right] = \frac{F\left[\text{N}\right] \times \rho\left[\text{g/cm}^3\right]}{\rho_L\left[\text{g/m}\right]} \tag{1}$$

From the constitutive stress-strain curves, the tangent modulus curve (E_t) can be derived by calculating the first derivative of stress with respect to strain, as shown in Equation 2. This parameter represents the instantaneous stiffness of the material at a given strain level. In addition to the complete curve profile, particular attention is given to extracting the maximum tangent modulus ($E_{t_{max}}$) along the curve and the tangent modulus at the rupture point ($E_{t_{rup}}$).

$$E_t = \frac{d\sigma}{d\varepsilon} \tag{2}$$

From the same constitutive stress-strain data, the secant modulus (E_s) can be calculated, defined as the slope of a straight line connecting the origin to a specific point of the stress-strain curve, as expressed in Equation 3. This parameter provides a measure of the mean stiffness of the material up to the chosen strain level.

$$E_s = \frac{\sigma}{\varepsilon} \tag{3}$$

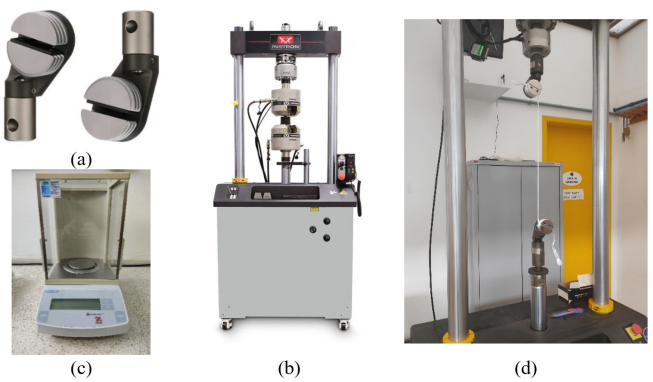

Figure 4. Equipment and rupture tests: (a) rope yarn grippers, interlace prevent slippage; (b) Instron 8801; (c) Ohaus Adventurer; (d) specimen fixed in the grips for rupture.

3. Results and Discussions

The data were filtered using boxplot analysis, resulting in the exclusion of 6 out of 140 individual rupture data points (≈4.3%). All groups demonstrated normal distribution and homogeneity of variance. The ANOVA tests further confirmed the findings that will be discussed later regarding the rupture force and strain after UV exposure in the HMPE and PET.

3.1 Rupture results after UV aging

The mean values of rupture force and rupture strain for each UV exposure time, along with their respective standard deviations, are presented in Table 3 for HMPE and PET. The same data are graphically represented in Figure 5 for HMPE and in Figure 6 for PET, allowing for a clearer visualization of the effects of UV exposure on the rupture force and rupture strain.

Table 3 shows that both fibers reach their highest rupture force in the unexposed condition. Figure 5 and Figure 6 highlight distinct behaviors under UV exposure: polyester exhibits a progressive decline in both rupture force and strain, while high-modulus polyethylene shows no statistically significant change.

To further interpret the data, values were normalized against the unexposed condition (0 days), enabling the calculation of percentage reductions for each exposure duration.

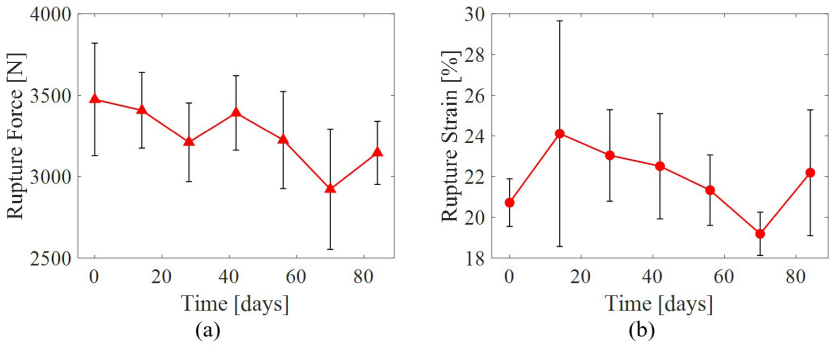

Figure 5. Rupture results after UV exposure on HMPE rope yarns: (a) mean rupture force and standard deviation; (b) mean rupture strain and standard deviation.

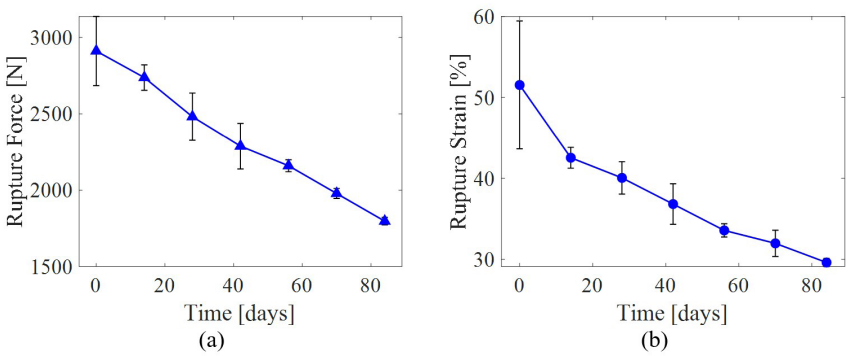

Figure 6. Rupture results after UV exposure on PET rope yarns: (a) mean rupture force and standard deviation; (b) mean rupture strain and standard deviation.

Table 3. Mean rupture results after ultraviolet exposure, HMPE and PET.

Time [days]	HMPE		PET	
	Force [N]	Strain [%]	Force [N]	Strain [%]
0	3473.94±345.80	20.72±1.17	2910.63±226.12	51.54±7.90
14	3407.32±232.74	24.11±5.54	2737.09±83.11	42.54±1.29
28	3210.43±242.04	23.04±2.25	2480.98±154.77	40.05±2.00
42	3391.21±228.91	22.51±2.59	2287.64±149.40	36.82±2.50
56	3224.43±298.54	21.33±1.73	2159.00±39.15	33.57±0.82
70	2922.34±368.86	19.19±1.06	1977.63±32.41	31.97±1.62
84	3145.73±194.09	22.19±3.09	1796.73±24.80	29.61±0.50

Normalized results reinforce the contrasting UV responses of HMPE and PET rope yarns. PET shows a monotonic decline in rupture force and strain, with reductions of 38.27% and 42.49%, respectively, after 84 days of exposure. HMPE, on the other hand, reaches its lowest values at 70 days, but with more moderate reductions: 15.88% in force and 7.38% in strain relative to the unexposed condition.

The experimental results reveal an unexpected behavior in HMPE rope yarns subjected to ultraviolet exposure, with upward fluctuations in mean rupture force and mean rupture strain even at longer exposure durations (Figure 5), contradicting the typical progressive degradation trend expected for these materials. These apparent gains occur within the overlap of standard deviations and were not statistically significant according to the applied tests (analysis of variance and post-hoc multiple comparison), suggesting they may stem from experimental scatter and intrinsic material variability.

At the same time, the trends suggested by the mean values cannot be overlooked. Possible hypotheses—requiring comparison with recent literature—include UV-induced surface crosslinking, relaxation of internal stresses, molecular rearrangement during exposure, minor moisture absorption effects, environmental fluctuations affecting mechanical response, and microstructural reorientation of fibers under combined effects[57-59]. In this context, the use of UV radiation for polymerization is well established under specific conditions. Decker[60] describes several UV-curing technologies, emphasizing kinetic aspects of ultrafast polymerization; Yin et al.[61] report improved mechanical properties in thermoplastic starch optimized by UV irradiation under wettability and hygroscopic conditions. For ultra-high molecular weight polyethylene (UHMWPE), Verma et al.[62] and Dong et al.[63] demonstrate mechanical enhancements from UV crosslinking, with indications of crystal packing formation and fiber shrinkage due to molecular disorientation. As crosslinking restricts molecular mobility, it can yield improved strength even after extended exposure.

Conversely, other studies report degradation consistent with the expected monotonic loss from UV aging, as seen in PET rope yarns results in the present study (Figure 6) and in Ainali et al.[64], that show UV-B irradiation reduces plasticity and causes gradual embrittlement. This contrast suggests that for HMPE, UV radiation may promote crosslinked structures via radiation energy absorption, bond scission, free radical generation, and subsequent new bond formation, altering molecular architecture and mechanical response. For PET, by contrast, results indicate no significant crosslinking, instead showing a gradual strength reduction without HMPE-like fluctuations. These considerations, although derived from mechanical results for HMPE and PET rope yarns, may guide future research across structural scales in offshore mooring systems, especially when physicochemical aspects of UV exposure are accounted for.

Curve fitting used only mean values and a literature-based script[55] testing linear, power, exponential, reciprocal, and Michaelis-Menten models. Using the coefficient of determination (R^2) to select the best fit, all graphs favored the linear model. For PET rope yarns, linear fitting showed good R^2 for both rupture force and strain. In contrast, HMPE's linear fit had a notably low R^2 despite being the best among the tested models.

For HMPE rope yarns, the rupture force fit yielded $R^2 \cong 0.625$ (Equation 4), while rupture strain showed a low $R^2 \cong 0.116$ (Equation 5). Both fitted models, alongside experimental data, are plotted in Figure 7.

$$F_{rup}\left[\mathrm{N}\right] \cong -4.9505 \times t\left[\mathrm{days}\right] + 3461.5 \tag{4}$$

$$\varepsilon_{rup}\left[\%\right] \cong -0.0182 \times t\left[\mathrm{days}\right] + 22.635 \tag{5}$$

For PET rope yarn samples, the fitted models performed excellently ($R^2 > 0.9$). Rupture force achieved $R^2 \cong 0.994$ (Equation 6), and rupture strain $R^2 \cong 0.928$ (Equation 7). Both models and their experimental data are shown in Figure 8.

$$F_{rup}\left[\mathrm{N}\right] \cong -13.221 \times t\left[\mathrm{days}\right] + 2890.9 \tag{6}$$

$$\varepsilon_{rup}\left[\%\right] \cong -0.2383 \times t\left[\mathrm{days}\right] + 48.022 \tag{7}$$

Due to the poor fit for HMPE, the equation coefficients lack interpretative value. In contrast, the strong fits for PET (high R^2) make the slope coefficients reliable indicators of degradation rates: rupture force declines by ≈13 N/day, and rupture strain by ≈0.24%/day.

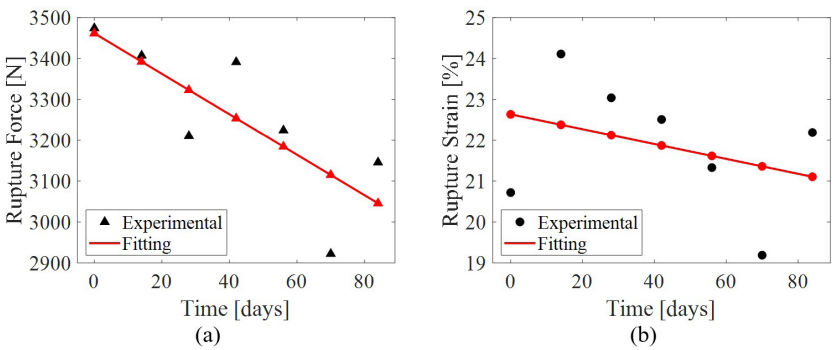

Figure 7. Curve fitting for rupture results after UV exposure on HMPE rope yarns: (a) fitting for mean rupture force; (b) fitting for mean rupture strain.

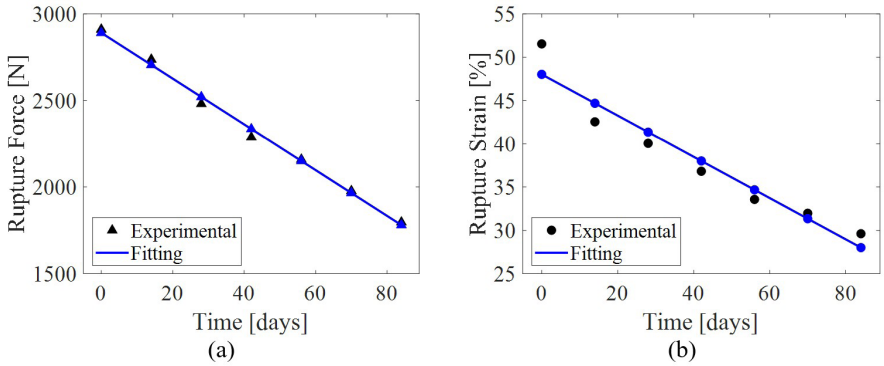

Figure 8. Curve fitting for rupture results after UV exposure on PET rope yarns: (a) fitting for mean rupture force; (b) fitting for mean rupture strain.

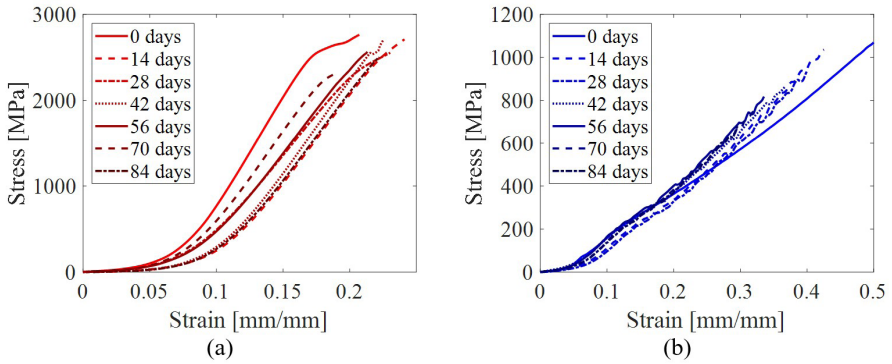

Figure 9. Constitutive rupture curves for rope yarns under UV conditions: (a) HMPE; (b) PET.

Table 4. Linear density and linear tenacity results, HMPE and PET.

Material	Rupture force [N]	Linear density [tex]	Linear tenacity [N/tex]
HMPE	3473.94±345.80	1220.08±3.10	2.847±0.291
PET	2910.63±226.12	3647.17±12.34	0.798±0.065

3.2 Effects on constitutive behavior

The rupture data in Section 3.1 refer to the final break point. However, as shown in Figure 5 and Figure 6, the force-strain curve shapes differ between HMPE and PET. Thus, plotting the full constitutive curve is relevant, as UV exposure may affect the material's behavior throughout the rupture process.

The constitutive curve, stress-strain terms, relies on stress calculations from Equation 1, which require fiber density—0.97 g/cm³ for HMPE and 1.38 g/cm³ for PET[10,15,40]—and linear density. For this reason, linear density tests were conducted. Combined with unexposed condition results, they provide the reference tenacity values listed in Table 4 for rope yarns.

Each UV exposure condition includes five rupture curves per material. However, aligning multiple experimental curves is challenging—particularly when computing pointwise first derivatives, which can introduce noise or discontinuities. Thus, a representative curve was selected for each condition and smoothed to reduce noise while preserving the constitutive behavior during rupture.

Figure 9a shows the constitutive curves for HMPE rope yarns under each UV exposure condition, while Figure 9b presents the corresponding curves for PET rope yarns.

The constitutive graphs represent raw experimental curves, which explains the visible oscillations—particularly in the PET curves (Figure 9b). Despite the reduction in rupture properties over time, PET yarns show nearly identical constitutive behavior across conditions, suggesting UV exposure primarily limits the extent of an otherwise consistent response. In contrast, HMPE curves show more variability, with some overlapping and others diverging significantly across exposure times in stress-strain behavior.

A notable aspect under constant extension rate loading is the material response at the multifilament level: HMPE typically shows near-linear behavior, while PET displays

initial curvature and changes along the stress-strain curve—consistent with literature reports[10,15,65]. However, in the curves obtained here, PET appears more linear and responsive than HMPE. In Figure 9b, PET shows only slight curvature near 50 MPa (≈5% of its ultimate stress), whereas HMPE (Figure 9a) exhibits a broader initial curvature extending to 400-500 MPa (≈20% of its ultimate stress).

3.3 Construction of tangent modulus curves and secant modulus curves

Despite smoothing, some variation is expected in the tangent modulus curves due to oscillations in the constitutive data. The goal is to analyze how the tangent modulus behaves across different regions of the curve. Using Equation 2, the tangent modulus is computed via numerical differentiation of the discrete experimental data, as shown in Equation 8, where E_{t_k} is the tangent modulus at the k-th data point, σ_k and σ_{k+1} are the stress values at points k and $k+1$, respectively, and ε_k and ε_{k+1} are the corresponding strain values. The index k refers to the position of the data point along the experimental curve.

$$E_{t_k} = \frac{\sigma_{k+1} - \sigma_k}{\varepsilon_{k+1} - \varepsilon_k} \tag{8}$$

Figure 10a shows the tangent modulus curves for HMPE rope yarns under each UV exposure condition, while Figure 10b presents the corresponding curves for PET rope yarns.

Figure 10 shows that HMPE's tangent modulus values are about four times higher than PET's. PET curves also exhibit greater oscillation, likely due to partial filament breaks causing small drops and recoveries from stress redistribution during rupture. For both fibers, the maximum tangent modulus occurs at the curve's start.

In the central region of HMPE tangent modulus curves (Figure 10a), a clear downward concavity appears across all UV exposures, with minimal noise or oscillation. Conversely, PET curves (Figure 10b) exhibit a generally constant modulus in this region but with significant oscillations, consistent with filament breakages and stress redistribution.

Maximum tangent modulus ($E_{t_{max}}$) and tangent modulus at rupture ($E_{t_{rup}}$) were obtained by numerically differentiating discrete stress-strain data. $E_{t_{max}}$ is the highest derivative value and sensitive to data acquisition frequency, so different sampling rates may affect results. $E_{t_{rup}}$ is calculated between the rupture point and its preceding data point. Table 5 shows these values for both HMPE and PET rope yarns.

The results are inconclusive behaviorally, likely because direct numerical differentiation is sensitive to experimental scatter caused by data acquisition rate and mechanical effects like partial filament breaks and stress redistribution. Future studies should consider alternative methods combining analytical and numerical approaches for adjustments to the tangent modulus analysis.

For the secant modulus curves, it is important to highlight their calculation using Equation 3, which, for a constitutive rupture dataset with k-th terms, takes the form presented in Equation 9, since the secant modulus is computed with respect to the origin $(\sigma_0, \varepsilon_0)$.

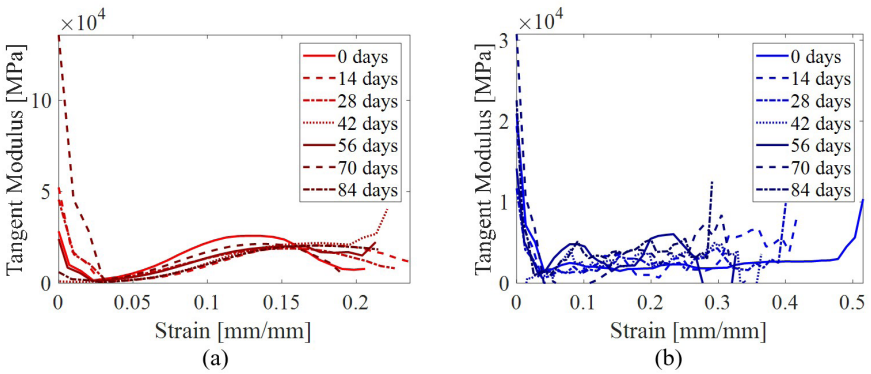

Figure 10. Tangent modulus curves in rupture for rope yarns under UV conditions: (a) HMPE; (b) PET.

Table 5. Maximum tangent modulus ($E_{t_{max}}$) and tangent modulus at rupture ($E_{t_{rup}}$) obtained from the tangent modulus curves for HMPE and PET rope yarns under UV conditions.

Time [days]	HMPE		PET	
	$E_{t_{max}}$ [MPa]	$E_{t_{rup}}$ [MPa]	$E_{t_{max}}$ [MPa]	$E_{t_{rup}}$ [MPa]
0	28304	7382	74854	10371
14	60151	12940	21735	986
28	45611	7745	13716	9934
42	4892200	24121	11745	1787
56	24103	22380	14411	3045
70	208790	4336	30732	4673
84	21219	11321	22582	1039

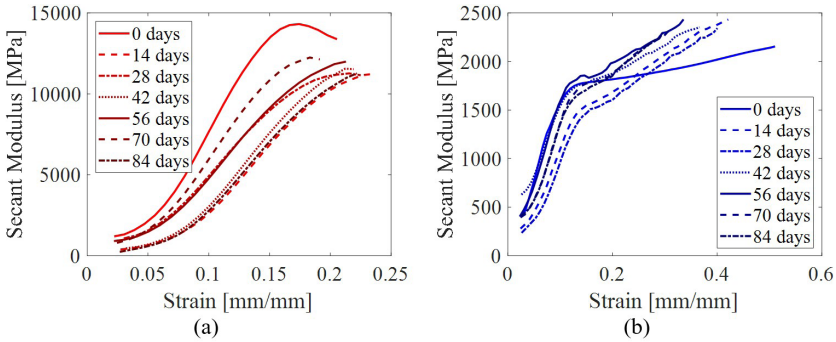

Figure 11. Secant modulus curves in rupture for rope yarns under UV conditions: (a) HMPE; (b) PET.

$$E_{s_k} = \frac{\sigma_k - \sigma_0}{\varepsilon_k - \varepsilon_0} = \frac{\sigma_k}{\varepsilon_k} \quad (9)$$

Accordingly, the secant modulus can be plotted as a function of strain, representing a mean measure of stiffness at each point, which accounts for the entire loading history, given that the calculation incorporates the cumulative stress and strain up to that k-th instant. These secant modulus curves are shown in Figure 11a for all UV exposure conditions of the HMPE rope yarns, and similarly in Figure 11b for the PET rope yarns.

The secant modulus curve was smoothed relative to the experimental data, removing initial points with E_s very high values tending toward infinity. Unlike the tangent modulus curves (which represent a measure of instantaneous stiffness between successive data points), the secant modulus curves (representing a mean stiffness) are quite stable, exhibiting minimal noise and a well-defined shape.

When comparing the secant modulus curves across materials, attention is drawn not only to the magnitude scale (HMPE rope yarns showing values approximately six times greater than PET rope yarns) but especially to the curve shape, which remains consistent for each material individually, even under different UV exposure conditions, but differs distinctly between the materials. HMPE rope yarns exhibit a smooth and progressive change in curvature, presenting a maximum secant modulus value that, at times, does not coincide with rupture due to a concavity change in the curve, Figure 11a. In contrast, PET rope yarns display two distinct regimes of monotonic tangent modulus increase: an initial segment with a steeper slope (higher rate) followed by a second segment characterized by a lower secant modulus gain rate (shallower slope), Figure 11b.

However, for both HMPE and PET, no clearly defined ordering of the secant modulus curves was observed as a function of UV exposure conditions, except for the non-exposed conditions, which for both materials exhibit behavior distinct from the other curves subjected to UV exposure (regardless of exposure duration).

4. Conclusions

This study investigated the effects of UV exposure on the mechanical behavior of synthetic rope yarns made of HMPE and PET used in offshore mooring systems. Using standardized tests, rigorous statistical filtering, and thorough analysis, the rupture force, rupture strain, and constitutive responses were comprehensively assessed. PET yarns showed a clear, monotonic decline in mechanical strength with increasing UV exposure, with strong linear correlations for both rupture force and rupture strain. In contrast, HMPE yarns exhibited only minor variations and no statistically significant degradation, despite some shifts in constitutive behavior.

The constitutive curves and tangent modulus analysis revealed distinct structural responses: PET exhibited more oscillations, likely due to internal filament failures, while HMPE maintained a more stable and consistent behavior. Although direct numerical differentiation offered insights into tangent modulus trends, its limitations suggest the need for refined analytical methods in future studies. Regarding the secant modulus, which represents a mean stiffness throughout the rupture test, the distinct curve shapes and magnitude differences between the two fiber types are noteworthy. However, no clear pattern was identified concerning the UV exposure conditions.

These results confirm HMPE's superior UV resistance compared to PET at the rope yarn scale—opposite to the typical behavior observed at the multifilament level, where PET is usually more UV stable and HMPE shows slight degradation. These findings, influenced by both UV exposure and sample type, provide valuable data for the design and lifetime assessment of synthetic mooring systems in offshore environments.

Future studies should consider the progression to other structural levels, longer ultraviolet exposure durations, and the inclusion of other fibers such as aramid and polyamide. Additionally, a more in-depth physicochemical analysis is needed to address the hypotheses raised in this work concerning the literature on surface cross-linking induced by UV radiation, which may contribute to mechanical improvement and strength even under prolonged UV exposure conditions (as observed for HMPE rope yarns)

5. Author's Contribution

- **Conceptualization** – Daniel Magalhães Da Cruz; Felipe Tempel Stumpf; Carlos Eduardo Marcos Guilherme; Ivan Napoleão Bastos; Ana Lúcia Nazareth da Silva

- **Data curation –** Daniel Magalhães Da Cruz; Marcelo de Ávila Barreto.
- **Formal analysis –** Daniel Magalhães Da Cruz.
- **Funding acquisition –** Larissa Basei Zangalli; Carlos Eduardo Marcos Guilherme; Ivan Napoleão Bastos.
- **Investigation –** Daniel Magalhães Da Cruz; Marcelo de Ávila Barreto; Ivan Napoleão Bastos.
- **Methodology –** Daniel Magalhães Da Cruz; Larissa Basei Zangalli; Carlos Eduardo Marcos Guilherme; Ivan Napoleão Bastos.
- **Project administration –** Felipe Tempel Stumpf; Carlos Eduardo Marcos Guilherme; Ivan Napoleão Bastos; Ana Lúcia Nazareth da Silva.
- **Resources –** Larissa Basei Zangalli; Felipe Tempel Stumpf; Carlos Eduardo Marcos Guilherme; Ivan Napoleão Bastos; Ana Lúcia Nazareth da Silva.
- **Software –** NA.
- **Supervision –** Carlos Eduardo Marcos Guilherme; Ivan Napoleão Bastos.
- **Validation –** Daniel Magalhães Da Cruz; Ivan Napoleão Bastos; Ana Lúcia Nazareth da Silva.
- **Visualization –** Daniel Magalhães Da Cruz; Ivan Napoleão Bastos; Ana Lúcia Nazareth da Silva.
- **Writing – original draft –** Daniel Magalhães Da Cruz.
- **Writing – review & editing –** Daniel Magalhães Da Cruz; Ivan Napoleão Bastos; Ana Lúcia Nazareth da Silva.

6. Acknowledgements

This study was financed in part by the Coordenação de Aperfeiçoamento de Pessoal de Nível Superior – Brasil (CAPES) – Finance Code 001 and Conselho Nacional de Desenvolvimento Científico e Tecnológico – CNPq [307889/2022], as well as the support of other funding agencies: Fundação de Amparo à Pesquisa do Estado do Rio Grande do Sul (FAPERGS), Fundação Carlos Chagas Filho de Amparo à Pesquisa do Estado do Rio de Janeiro (FAPERJ), and Financiadora de Estudos e Projetos (Finep).

We are also grateful for the financial support provided by the company Tecnofibers Desenvolvimento e Tecnologia Ltda. The authors also want to express the eternal thanks to Milton Briguet Bastos (*in memorian*).

7. References

1. Del Vecchio, C. J. M. (1992). *Light weight materials for deep water moorings* (Doctoral dissertation). University of Reading, Reading.
2. Winkler, M. M., & McKenna, H. A. (1995). *The polyester rope taut leg mooring concept: a feasible means for reducing deepwater mooring cost and improving stationkeeping performance.* In *Offshore Technology Conference*. Houston: OTC. http://doi.org/10.4043/7708-MS
3. Ma, W., Huang, K., Lee, M.-Y., Albuquerque, S., & Palazzo, F. G. (1999). *On the design and installation of an innovative deepwater taut-leg mooring system.* In *Offshore Technology Conference*. Houston: OTC. http://doi.org/10.4043/10780-MS
4. Wibner, C., Versavel, T., & Masetti, I. (2003). *Specifying and testing polyester mooring rope for the Barracuda and Caratinga FPSO deepwater mooring systems.* In *Offshore Technology Conference*. Houston: OTC. http://doi.org/10.4043/15139-MS
5. McKenna, H. A., Hearle, J. W. S., & O'Hear, N. (2004). *Handbook of fibre rope technology*. Sawston: Woodhead publishing.. http://doi.org/10.1533/9781855739932.
6. Flory, J. F., Banfield, S. J., & Berryman, C. (2007). *Polyester mooring lines on platforms and MODUs in deep water.* In *Offshore Technology Conference*. Houston: OTC. http://doi.org/10.4043/18768-MS
7. Rossi, R., Del Vecchio, C. J., & Gonçalves, R. C. F. (2010). *SS: fiber moorings, recent experiences and research: moorings with polyester ropes in Petrobras: experience and the evolution of life cycle management.* In *Offshore Technology Conference*. Houston: OTC. http://doi.org/10.4043/20845-MS
8. Davies, P., Bouquet, P., Conte, M., & Deuff, A. (2006). *Tension/torsion behavior of deepwater synthetic mooring lines.* In *Offshore Technology Conference*. Houston: OTC. http://doi.org/10.4043/17872-MS
9. Haach, L. F., Bastos, M. B., & Poitevin, D. T. (2010). *Prospects of synthetic fibers for deepwater mooring.* In *Proceedings of the Rio Oil and Gas Expo and Conference*. Rio de Janeiro: Instituto Brasileiro de Petróleo, Gás e Biocombustíveis.
10. Bastos, M. B., & Silva, A. L. N. (2020). *Evaluating offshore rope fibers: impact on mooring systems integrity and performance.* In *Offshore Technology Conference*. Houston: OTC. http://doi.org/10.4043/30830-MS
11. Bastos, M. B. (2013). *Improved high tenacity/high modulus polyester for stiffer mooring ropes.* In *2013 MTS/IEEE OCEANS-Bergen*. Bergen: Institute of Electrical and Electronics Engineers. http://doi.org/10.1109/OCEANS-Bergen.2013.6607949.
12. Silva, T. N., Sousa, A. M. F., Silva, A. L. N., Passos, A. A., & Pacheco, E. B. A. V. (2025). Yarn production from the offshore industry mooring rope waste: a circular textile economy opportunity. *Journal of Polymers and the Environment*, *33*(1), 197-209. http://doi.org/10.1007/s10924-024-03414-2.
13. Huang, W. (2026). Research directions in synthetic fiber ropes applied as mooring lines for floating offshore wind turbines. *Renewable & Sustainable Energy Reviews*, *225*, 116183. http://doi.org/10.1016/j.rser.2025.116183.
14. El Nemr, A. (2012). *From natural to synthetic fibers.* In A. El Nemr (Ed.), *Textiles: types, uses and production methods* (pp. 1-152). New York: Nova Science Publishers.
15. Weller, S. D., Johanning, L., Davies, P., & Banfield, S. J. (2015). Synthetic mooring ropes for marine renewable energy applications. *Renewable Energy*, *83*, 1268-1278. http://doi.org/10.1016/j.renene.2015.03.058.
16. Da Cruz, D. M., Zangalli, L. B., Barreto, M. A., Silva, A. L. N., & Bastos, I. N. (2024). *Offshore mooring challenges for FOWT systems and MRE devices: synthetic fiber solutions for mooring ropes.* In *ROG.e 2024*. Rio de Janeiro: Instituto Brasileiro de Petróleo e Gás. http://doi.org/10.48072/2525-7579.roge.2024.3210.
17. Chevillotte, Y., Marco, Y., Bles, G., Devos, K., Keryer, M., Arhant, M., & Davies, P. (2020). Fatigue of improved polyamide mooring ropes for floating wind turbines. *Ocean Engineering*, *199*, 107011. http://doi.org/10.1016/j.oceaneng.2020.107011.
18. Sørum, S. H., Fonseca, N., Kent, M., & Faria, R. P. (2023). Assessment of nylon versus polyester ropes for mooring of floating wind turbines. *Ocean Engineering*, *278*, 114339. http://doi.org/10.1016/j.oceaneng.2023.114339.
19. Kamizawa, K., Yoshimoto, H., & Chujo, T. (2024). *The Field Test of a Shallow-Water Mooring System for FOWT Using Nylon Synthetic Fiber Ropes.* In *International Conference on Offshore Mechanics and Arctic Engineering*. Singapore: The American Society of Mechanical Engineers. http://doi.org/10.1115/OMAE2024-126265

20. Hearle, J. W. S. (Ed.) (2001). *High-performance fibres*. Amsterdam: Elsevier.
21. Chi, C.-H., Lundhild, E. M., Veselis, T., & Huntley, M. (2009). *Enabling ultra-deepwater mooring with aramid fiber rope technology.* In *Offshore Technology Conference*. Houston: OTC. http://doi.org/10.4043/20074-MS
22. García, J. M., García, F. C., Serna, F., & de la Peña, J. L. (2010). High-performance aromatic polyamides. *Progress in Polymer Science*, *35*(5), 623-686. http://doi.org/10.1016/j.progpolymsci.2009.09.002.
23. Vlasblom, M., Boesten, J., Leite, S., & Davies, P. (2012). *Creep and stiffness of HMPE fiber for permanent deepwater offshore mooring.* In *2012 Oceans-Yeosu*. Yeosu: Institute of Electrical and Electronics Engineers. http://doi.org/10.1109/OCEANS-Yeosu.2012.6263399.
24. Ja'e, I. A., Ali, M. O. A., Yenduri, A., Nizamani, Z., & Nakayama, A. (2022). Effect of various mooring materials on hydrodynamic responses of turret-moored FPSO with emphasis on intact and damaged conditions. *Journal of Marine Science and Engineering*, *10*(4), 453. http://doi.org/10.3390/jmse10040453.
25. Lian, Y., Zhang, B., Ji, J., Pan, Z., Jiang, T., Zheng, J., Ma, G., Zhu, Z., Zhu, Z., & Chen, W. (2023). Experimental investigation on service safety and reliability of full-scale HMPE fiber slings for offshore lifting operations. *Ocean Engineering*, *285*(Part 2), 115447. http://doi.org/10.1016/j.oceaneng.2023.115447.
26. Pasternak, J., Fronzaglia, B., Garrity, R., Gilmore, J., & Heyl, C. (2024). *Deployment and Testing of HMPE Rope for Long-Term Moorings.* In *Offshore Technology Conference*. Houston: OTC. http://doi.org/10.4043/35375-MS
27. Bosman, R., Zhang, Q., Leao, A., & Godreau, C. (2020). *First class certification on HMPE fiber ropes for permanent floating wind turbine mooring system.* In *Offshore Technology Conference*. Houston: OTC. http://doi.org/10.4043/30475-MS
28. Da Cruz, D. M., Barreto, M. A., Zangalli, L. B., Popiolek, T. L. Jr., & Guilherme, C. E. M. (2023). *Experimental study of creep behavior at high temperature in different HMPE fibers used for offshore mooring.* In *Offshore Technology Conference Brasil*. Rio de Janeiro: OTC. http://doi.org/10.4043/32760-MS.
29. Liu, H., Huang, W., Lian, Y., & Li, L. (2014). An experimental investigation on nonlinear behaviors of synthetic fiber ropes for deepwater moorings under cyclic loading. *Applied Ocean Research*, *45*, 22-32. http://doi.org/10.1016/j.apor.2013.12.003.
30. Weller, S. D., Davies, P., Vickers, A. W., & Johanning, L. (2015). Synthetic rope responses in the context of load history: the influence of aging. *Ocean Engineering*, *96*, 192-204. http://doi.org/10.1016/j.oceaneng.2014.12.013.
31. Mackay, T., & Ridge, I. M. (2022). Abrasion testing of fibre rope on impermeable fabrics for wave energy converter systems. *Renewable Energy*, *201*(Part 1), 993-1009. http://doi.org/10.1016/j.renene.2022.11.052.
32. Li, W., Liu, X., Li, G., Lin, S., Li, H., & Ge, Y. (2023). Temperature and humidity effects on the dynamic stiffness of a polyester mooring rope. *Journal of Marine Science and Engineering*, *11*(1), 91. http://doi.org/10.3390/jmse11010091.
33. Da Cruz, D. M., Melito, I., Cruz, A. J. Jr., Bastos, I. N., Silva, A. L. N., Vassoler, J. M., Clain, F. M., & Guilherme, C. E. M. (2024). Assessment of mechanical degradation in polyester fibers for offshore mooring through hydrolysis processes in seawater. *Macromolecular Symposia*, *413*(6), 2400097. http://doi.org/10.1002/masy.202400097.
34. Vaseghi, R. (2004). *A new method of termination for heavy-duty synthetic rope fibres* (Doctoral dissertation). Bournemouth University, Bournemouth.
35. Bao, J., Hu, W., Gao, Y., & Lu, Z. (2024). Review of rope coating research: mechanism, application, and future directions. *Textile Research Journal*, *95*(11-12), 1468-1485. http://doi.org/10.1177/00405175241289567.
36. Davies, P., Lacotte, N., Fourestier, G., & Petton, I. (2025). Mechanical performance after service of hybrid synthetic mooring lines for weather buoys. *Applied Ocean Research*, *154*, 104366. http://doi.org/10.1016/j.apor.2024.104366.
37. Said, M. A., Dingwall, B., Gupta, A., Seyam, A. M., Mock, G., & Theyson, T. (2006). Investigation of ultra violet (UV) resistance for high strength fibers. *Advances in Space Research*, *37*(11), 2052-2058. http://doi.org/10.1016/j.asr.2005.04.098.
38. Flory, J. F., & Banfield, S. J. (2011). *Fiber rope myths.* In *OCEANS'11 MTS/IEEE KONA*. Waikoloa: Institute of Electrical and Electronics Engineers. http://doi.org/10.23919/OCEANS.2011.6106929.
39. Sørensen, L., Groven, A. S., Hovsbakken, I. A., Del Puerto, O., Krause, D. F., Sarno, A., & Booth, A. M. (2021). UV degradation of natural and synthetic microfibers causes fragmentation and release of polymer degradation products and chemical additives. *The Science of the Total Environment*, *755*(Pt 2), 143170. http://doi.org/10.1016/j.scitotenv.2020.143170. PMid:33158534.
40. Da Cruz, D. M., Stumpf, F. T., Vassoler, J. M., & Guilherme, C. E. M. (2024). Assessment of the effects of UV-A exposure on the mechanical strength of offshore mooring multifilaments. *Acta Polytechnica*, *64*(6), 487-500. http://doi.org/10.14311/AP.2024.64.0487.
41. Del Vecchio, C., Yan, H., Rieth, D., Gabrielsen, Ø., Menezes, F., Jegannathan, M., Oliveira, A. C., & Gomes, J. (2024). *Advances towards replacing top chain with fiber rope for offshore moorings: a Deepstar study.* In *Offshore Technology Conference*. Houston: OTC. http://doi.org/10.4043/35339-MS
42. Da Cruz, D. M., Penaquioni, A., Zangalli, L. B., Bastos, M. B., Bastos, I. N., & Silva, A. L. N. (2023). Non-destructive testing of high-tenacity polyester sub-ropes for mooring systems. *Applied Ocean Research*, *134*, 103513. http://doi.org/10.1016/j.apor.2023.103513.
43. Belloni, E. S., Clain, F. M., & Guilherme, C. E. M. (2021). Post-impact mechanical characterization of HMPE yarns. *Acta Polytechnica*, *61*(3), 406-414. http://doi.org/10.14311/AP.2021.61.0406.
44. Da Cruz, D. M., Clain, F. M., & Guilherme, C. E. M. (2022). Experimental study of the torsional effect for yarn break load test of polymeric multifilaments. *Acta Polytechnica*, *62*(5), 538-548. http://doi.org/10.14311/AP.2022.62.0538.
45. International Organization for Standardization – ISO. (2020). *ISO 18692-3:2020: Fibre ropes for offshore stationkeeping — Part 3: High modulus polyethylene (HMPE).* Geneva: ISO. Retrieved in 2025, May 31, from https://www.iso.org/standard/77487.html
46. International Organization for Standardization – ISO. (2019). *ISO 18692-2:2019: Fibre ropes for offshore stationkeeping - Part 2: Polyester*. Geneva: ISO. Retrieved in 2025, May 31, from https://www.iso.org/standard/70290.html
47. Q-Lab Corporation. (2006). *Technical bulletin LU-8160.* Cleveland: Q-Lab Corporation. Retrieved in 2025, May 31, from http://www.q-lab-corporation.ru/doc/QUV-LU-8160_web.pdf
48. International Organization for Standardization – ISO. (2009). *ISO 2062:2009: Textiles — Yarns from packages — Determination of single-end breaking force and elongation at break using constant rate of extension (CRE) tester.* Geneva: ISO. Retrieved in 2025, May 31, from https://www.iso.org/standard/45642.html

49 American Society for Testing and Materials – ASTM. (2018). *ASTM D1577-07:2018: standard test methods for linear density of textile fibers.* West Conshohocken: ASTM. http://doi.org/10.1520/D1577-07R18.

50. International Organization for Standardization – ISO. (2005). *ISO 139:2005: Textiles — Standard atmospheres for conditioning and testing.* Geneva: ISO. Retrieved in 2025, May 31, from https://www.iso.org/standard/35179.html

51. John, P. W. M. (1990). *Statistical methods in engineering and quality assurance.* Hoboken: John Wiley & Sons, Inc. http://doi.org/10.1002/9780470316825
52. Peng, Z., Wang, X., & Wu, Z. (2024). Statistical modeling and reliability analysis of large-scale multi-tendon fiber-reinforced polymer cables. *Engineering Structures*, *300*, 117226. http://doi.org/10.1016/j.engstruct.2023.117226.
53. Boiko, Y. M., Marikhin, V. A., & Myasnikova, L. P. (2023). Tensile strength statistics of high-performance mono-and multifilament polymeric materials: on the validity of normality. *Polymers*, *15*(11), 2529. http://doi.org/10.3390/polym15112529. PMid:37299329.
54. Orange. (2025). *Orange: Data mining toolbox in Python.* Ljubljana: Orange. Retrieved in 2025, May 31, from https://orangedatamining.com/
55. Da Cruz, D. M., Melito, I., Cruz Júnior, A. J., Sales, M. W. R., Popiolek Júnior, T. L., & Guilherme, C. E. M. (2024). Desenvolvimento de código aberto em Octave para ajustes de funções através de linearização e MMQ. *Engineering and Science*, *13*(1), 1-14. http://doi.org/10.18607/ES20241316896.
56. Melito, I., Da Cruz, D. M., Belloni, E. S., Clain, F. M., & Guilherme, C. E. M. (2023). The effects of mechanical degradation on the quasi static and dynamic stiffness of polyester yarns. *Engineering Solid Mechanics*, *11*(3), 243-252. http://doi.org/10.5267/j.esm.2023.4.001.
57. Iacopi, F., Travaly, Y., Eyckens, B., Waldfried, C., Abell, T., Guyer, E. P., Gage, D. M., Dauskardt, R. H., Sajavaara, T., Houthoofd, K., Grobet, P., Jacobs, P., & Maex, K. (2006). Short-ranged structural rearrangement and enhancement of mechanical properties of organosilicate glasses induced by ultraviolet radiation. *Journal of Applied Physics*, *99*(5), 053511. http://doi.org/10.1063/1.2178393.
58. Scott, T. F., Draughon, R. B., & Bowman, C. N. (2006). Actuation in crosslinked polymers via photoinduced stress relaxation. *Advanced Materials*, *18*(16), 2128-2132. http://doi.org/10.1002/adma.200600379.
59. Ramachandran, D., & Urban, M. W. (2011). Sensing macromolecular rearrangements in polymer networks by stimuli-responsive crosslinkers. *Journal of Materials Chemistry*, *21*(23), 8300-8308. http://doi.org/10.1039/c0jm03722b.
60. Decker, C. (1998). The use of UV irradiation in polymerization. *Polymer International*, *45*(2), 133-141. http://doi.org/10.1002/(SICI)1097-0126(199802)45:2<133::AID-PI969>3.0.CO;2-F.
61. Yin, P., Chen, C., Ma, H., Gan, H., Guo, B., & Li, P. (2020). Surface cross-linked thermoplastic starch with different UV wavelengths: mechanical, wettability, hygroscopic and degradation properties. *RSC Advances*, *10*(73), 44815-44823. http://doi.org/10.1039/D0RA07549C. PMid:35516245.
62. Verma, N., Pathak, H., Keshri, A. K., Prasad, A., & Zafar, S. (2022). Influence of UV exposure on mechanical behavior and cellular compatibility of nano-hydroxyapatite reinforced ultra-high molecular weight polyethylene. *Materials Today. Communications*, *31*, 103542. http://doi.org/10.1016/j.mtcomm.2022.103542.
63. Dong, T., Niu, F., Qiang, Z., Wang, X., Guo, J., Wang, Y., & He, Y. (2024). Thermal aging behavior and heat resistance mechanism of ultraviolet crosslinked ultra-high molecular weight polyethylene fiber. *Journal of Applied Polymer Science*, *141*(28), e55648. http://doi.org/10.1002/app.55648.
64. Ainali, N. M., Bikiaris, D. N., & Lambropoulou, D. A. (2021). Aging effects on low-and high-density polyethylene, polypropylene and polystyrene under UV irradiation: an insight into decomposition mechanism by Py-GC/MS for microplastic analysis. *Journal of Analytical and Applied Pyrolysis*, *158*, 105207. http://doi.org/10.1016/j.jaap.2021.105207.
65. Da Cruz, D. M., Popiolek Júnior, T. L., Barreto, M. A., Souza, S. P., Zangalli, L. B., Cruz Júnior, A. J., Martins, T. C., Silva, A. L. N., Bastos, I. N., & Guilherme, C. E. M. (2024). Numerical simulation with hyperelastic constitutive model for high-performance multifilaments used in offshore mooring ropes. *The Journal of Engineering and Exact Sciences*, *10*(2), 17255. http://doi.org/10.18540/jcecvl10iss2pp17255.

Received: May 31, 2025
Revised: Aug. 12, 2025
Accepted: Aug. 20, 2025

Editor-in-Chief: Sebastião V. Canevarolo